

# Preparation of thorium dioxide nanofibers by electrospinning

Vojtech Kundrat<sup>a</sup>, Zdenek Moravec<sup>a</sup>, Jiri Pinkas<sup>a, b, \*</sup>

<sup>a</sup> Masaryk University, Department of Chemistry, Kotlarska 2, CZ-61137, Brno, Czech Republic

<sup>b</sup> CEITEC MU, Masaryk University, Kamenice 5, CZ-62500, Brno, Czech Republic



## ARTICLE INFO

### Article history:

Received 14 January 2020

Received in revised form

5 April 2020

Accepted 6 April 2020

Available online 14 April 2020

### Keywords:

Electrospinning

Thorium dioxide

Thoria

Nanofibers

Polyvinylpyrrolidone

Polyvinyl alcohol

## ABSTRACT

For the first time, we report the preparation of thorium dioxide with nanofibrous morphology by the electrospinning method. Two approaches were employed with different electrospun solution compositions and inorganic precursors. Thorium nitrate with polyvinyl alcohol (PVA) as a supporting polymer was successfully electrospun from an aqueous solution resulting in green composite fibers that were calcined at 773 K to pure ThO<sub>2</sub> nanofibers of diameter  $76 \pm 25$  nm. Another precursor solution was based on organic solvents and thorium acetylacetonate complex with polyvinylpyrrolidone (PVP). Green fibers were calcined at 673 K to porous nanofibers of ThO<sub>2</sub> with an average diameter of  $34 \pm 18$  nm and surface area of  $85 \text{ m}^2 \text{ g}^{-1}$ . The prepared materials were characterized by TGA-DSC, SEM, TEM, PXRD, and BET methods.

© 2020 Elsevier B.V. All rights reserved.

## 1. Introduction

Thorium dioxide, thoria, is a well-known material with an extended application history in the form of gas mantles for Auer lanterns [1]. Thoria forms a single polymorph that crystallizes in the face-centered cubic lattice and belongs to the fluorite family. The melting point of thoria at 3631 K is the highest of all oxides [2,3]. Thorium dioxide is weakly radioactive due to the presence of thorium isotopes, mainly <sup>232</sup>Th (99.98%) with a very long half-life ( $1.4 \times 10^{10}$  years). Thorium dioxide found its use in nuclear reactors as a fertile component of mixed-oxide fuels [4,5]. Thoria-based fuels will be used in Advanced Heavy Water Reactors [6], and it is also used as a blanket material in Fast Breeder Reactors [7]. Thoria is also employed in special optical glasses, in refractory ceramic materials [8], in welding rods for tungsten workup [9], and potentially as composite heterogeneous catalysts [10–12].

Nanocrystalline particles and nanoparticles found applications in many areas. They could be used as precursors for obtaining ultrafine ceramics. Produced materials have superior properties and can be prepared under milder conditions than in traditional approaches. Denser materials could be obtained by a nanoprecursor

route due to the higher interparticle stress and smaller initial grains, moreover, by using lower sintering temperatures [13–15]. Production of metal oxide nanoparticles could be achieved by gas-phase methods including aerosol-based processes, for example fumed silica or titania from tetrachloride precursors by vapor phase oxidation [16]. Also, liquid-phase processes could be used, e.g., classical methods of sol-gel synthesis, hydrothermal or generally solvothermal reactions, sonochemical processes, and other various types of preparations [17]. Every mentioned method is characterized by its advantages and final material properties; however, a general issue in all nanoparticle systems is the same, i.e., a tendency to agglomerate, in some cases penetration of biological membranes, and relatively difficult handling properties [18]. In comparison nanofibers, even calcined ones, act as bulk objects therefore are easily and relatively safely handled; however, when broken, ground or pulverized this benefit may disappear.

Preparation of nanocrystalline thoria is a field of interest due to the direct application of prepared materials in powder sintering and preparation of potentially superior materials for nuclear fuel, catalysis, and many other fields. An array of preparation routes have been tested, and a substantial body of work has been reported on electrochemical precipitation [19], sol-gel technique [20,21], thin-film preparation by sputtering [22], aerogel formation [23], citrate Pechini process [24], combustion methods [25], thermal decomposition of nitrate [26] and oxalate [27], microwave decomposition

\* Corresponding author. Masaryk University, Department of Chemistry, Kotlarska 2, CZ-61137, Brno, Czech Republic.

E-mail address: [jpinkas@chemi.muni.cz](mailto:jpinkas@chemi.muni.cz) (J. Pinkas).

**Table 1**  
Electrospinning parameters.

Solution	High voltage (+) [kV]	High voltage (-) [kV]	Flow rate [ $\mu\text{l min}^{-1}$ ]	Electrode distance [cm]
A aqueous/ $\text{Th}(\text{NO}_3)_4$	$15.0 \pm 0.1$	$-10 \pm 0.1$	10	15
B organic/ $\text{Th}(\text{acac})_4$	$15.0 \pm 0.1$	0*	100	15

\*- collector was grounded.

**Table 2**  
Characteristics of electrospinning solutions.

Solution parameter	A - aqueous/ $\text{Th}(\text{NO}_3)_4$	B - organic/ $\text{Th}(\text{acac})_4$
Dynamic viscosity [mPa s]	$375.9 \pm 1.2$	$15.5 \pm 0.3$
Conductivity [ $\mu\text{S cm}^{-1}$ ]	$22.4 \pm 0.1 \times 10^3$	$52 \pm 1$
Surface tension [ $\text{mN m}^{-1}$ ]	$75 \pm 4$	$24 \pm 3$

[28], hydrothermal approach [29–31], and non-aqueous solution thermolysis [32,33].

Electrospinning is an efficient method of production sub-micrometric and nanoscopic fibers from various materials, including inorganic ceramic compounds [34–37]. A laboratory electrospinning set-up in its simplest form is composed of a syringe pump, a syringe with a metallic needle, a high voltage power source, and a collector [38]. Electrospinning is a process of mass transport from the tip of the needle filled with a spinning solution towards the grounded or negatively charged collector induced by a high-voltage electric field. The solvent evaporates from the liquid jet during the flight, and the fibers are then collected in the form of nonwoven textiles. Inorganic fibers are obtained by calcination of a green composite of supporting organic polymer and inorganic precursor. The high-temperature treatment removes the organic phase, and in an ideal case, only ceramic fibers are left. Further treatment could involve, for example, reduction or oxidation in a proper atmosphere. However, the overall process is influenced from the beginning mainly by the selection of a spinning solution, its composition, and in case of inorganic materials mainly by the form of the inorganic precursor.

In the case of thoria, the widely used precursors are thorium nitrate pentahydrate or tetrahydrate, which are readily soluble in aqueous solvents. Electrospinning from aqueous solutions is possible; however, a low evaporation rate and a high surface tension of polymer solutions are not favorable for obtaining a highly productive process. Because of these limitations, organic solutions are introduced; however, different inorganic precursors have to be applied because of solubility issues in organic solvents. From that point of view, thorium acetylacetonate is a viable precursor as it is easily produced by precipitation in basic conditions [39] and soluble in many organic solvents.

Here we present for the first time the preparation of thorium dioxide polycrystalline nanofibers by the electrospinning method from two principally different solutions, aqueous and organic, with two different precursors. The prepared fibers were characterized by TGA-DSC, SEM, TEM, PXRD, and BET methods.

## 2. Experimental

### 2.1. Materials and methods

Thorium nitrate tetrahydrate,  $\text{Th}(\text{NO}_3)_4 \cdot 4\text{H}_2\text{O}$ , (99.8%) was obtained from Lachema (CZ) and used in a hydrated form as received. Thorium acetylacetonate,  $\text{Th}(\text{acac})_4$ , was prepared according to the literature [39]. Polyvinyl alcohol (PVA, Mowiol 18–88) and Polyvinylpyrrolidone (PVP,  $M_w = 360$  kDa) were obtained from Merck and used as received. Acetone and ethanol (absolute) were

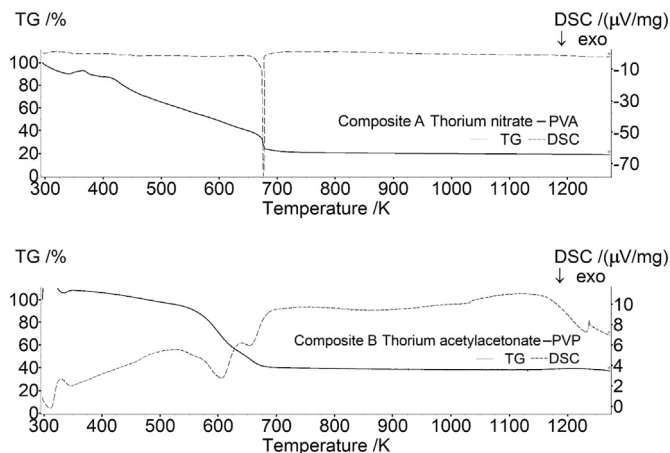


**Fig. 1.** TGA/DSC measurements of green composites from solutions A (top) and B (bottom).

purchased from Penta Chemicals (CZ) in a p.a. quality and used without further workup.

A custom designed, lab scale electrospinning set-up consisting of two power sources, positive and negative, capable of delivering 0–25 kV and –15 to 0 kV, respectively, a syringe pump (New Era Scientific), a plastic syringe with a metallic needle (diameter of 1 mm), and a round collector (diameter of 200 mm) [37]. The positive power source output was attached to the metallic needle, and the negative one was connected to the collector. Electrospinning was performed in a fume hood and air-conditioned room with stable relative humidity set at 40% and temperature 23 °C. The settings of electrospinning variables for the two precursor solutions are shown in Table 1.

Two solutions were prepared for electrospinning and characterized by viscosimetry, conductometry, and surface tension measurement.

#### Solution A

PVA (0.4 g) was dissolved in hot deionized water (4.6 g), and after cooling down,  $\text{Th}(\text{NO}_3)_4 \cdot 4\text{H}_2\text{O}$  (0.4 g) was added and dissolved. The solution was stirred for 1 h at ambient temperature. A clear solution was formed and characterized.

#### Solution B

PVP (0.5 g) was dissolved in ethanol (9 g) by stirring for 1 h.  $\text{Th}(\text{acac})_4$  (0.5 g, acac = acetylacetonate) was dissolved in acetone (5 g) by stirring for a few minutes. After complete dissolution, the thorium-containing solution was added by a syringe to the stirred solution of the polymer. A clear solution was formed and characterized.

### 2.2. Characterization of electrospinning solutions and prepared fibers

The prepared solutions A and B were characterized by conductometry, viscosimetry, and surface tension measurements. The electrical conductivity of solutions was obtained on a Cond51 conductometer from XS Instruments. Viscosity measurement was

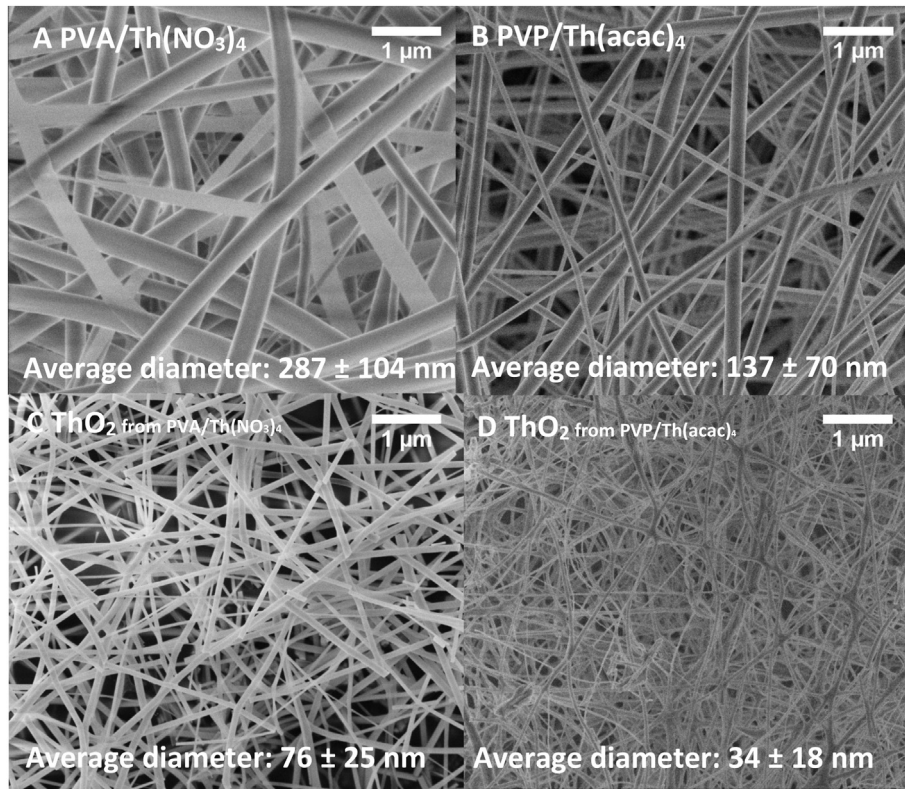


**Fig. 2.** SEM micrographs of green composites (A, B) and calcined fibers (C, D) produced from PVA/Th(NO<sub>3</sub>)<sub>4</sub> (A, C) and PVP/Th(acac)<sub>4</sub> (B, D).

performed on an Alpha Fungilab rotational viscosimeter. Surface tension was obtained on a Sigma 700 tensiometer with a Wilhelmy probe. Obtained values for both solutions are presented in Table 2.

By electrospinning, a green fibrous composite of an inorganic precursor and organic polymer was formed. The fiber mat was collected on aluminum foil and peeled off. The next step was calcination of the prepared materials, which was performed in a muffle oven under an air atmosphere. The green fibers made from solution A and B were calcined at a temperature of 773 K and 673 K, respectively. In all cases, the heating rate was set to 4 h to achieve the maximum calcination temperature then followed by another 4 h at a constant temperature and finished by spontaneous cooling down to ambient temperature. After heat treatments, calcined materials were collected and analyzed.

The prepared nanofibrous materials were characterized by scanning electron microscopy (SEM) and transmission electron microscopy (TEM). Samples for the TEM measurements were dispersed in methanol, and 4 μl of the suspension was placed on a Quantifoil copper grid and allowed to dry by evaporation at ambient temperature. TEM characterizations were performed on the FEI Tecnai G2 microscope at 200 kV equipped with a 4k CCD camera FEI Eagle. Images were analyzed by the ImageJ software for the fiber diameter and size distribution. Thermogravimetric and differential scanning calorimetry (TGA/DSC) analysis was performed on a Netzsch Jupiter STA 449 instrument with a heating rate of 10 K min<sup>-1</sup> and the maximum temperature of 1273 K. The PXRD measurements were performed on a GNR Europe 600 diffractometer with a Co ( $\lambda_{K\alpha} = 1.79030 \text{ \AA}$ ) X-ray lamps. The specific surface area was determined by the BET method using nitrogen as gaseous adsorbate performed on a Quantachrome Autosorb-1MP porosimeter. Pore size distributions were obtained using the density functional theory (DFT) method [40,41]. The kernel for N<sub>2</sub> at 77 K on silica (cylindrical pore, NLDFT equilibrium model), linear scale, and

bin pore width of 0.500 Å were used.

### 3. Results and discussion

For the primary evaluation of the preparation of thoria nanofibers, two solutions were tested based on a different approach from the solvent and precursor point of view. Thorium nitrate is the most frequently used precursor for thoria preparation; therefore, it was used as a starting material together with water-soluble polyvinyl alcohol, which is an optimal supporting polymer for electrospinning [42–44]. The prepared solution A had high conductivity due to the presence of dissociated ions and quite a high surface tension and viscosity due to the dissolved polymer. The second solution B was based on an organic solvent (ethanol/acetone) and PVP as a well-spinnable polymer [45–47]. Thorium acetylacetonate complex is easily soluble in organic solvents and served as an inorganic precursor. Simple mixing and dissolving of components of solution B in one vessel were found challenging because of incomplete dissolution and precipitation, which was observed as white turbidity in the solution. However, the slow mixing of prepared solutions (PVP in ethanol and Th(acac)<sub>4</sub> in acetone) produced a transparent and slightly yellow homogeneous mixture. The main difference between aqueous and organic solutions is in their conductivity and dynamic viscosity. The organic solution had substantially lower values in both parameters. Also, the surface tension is three times lower than for the aqueous solution. Together with its high evaporation rate, it results in the substantially different properties of the solutions, which is evidenced in the electrospinning process itself. For successful jet formation, a higher voltage has to be used in the case of the aqueous solution to overcome the surface tension. In the case of the organic solution, it is possible to use a ten times higher feed rate without dripping of surplus solution (Table 1), which means increased productivity of

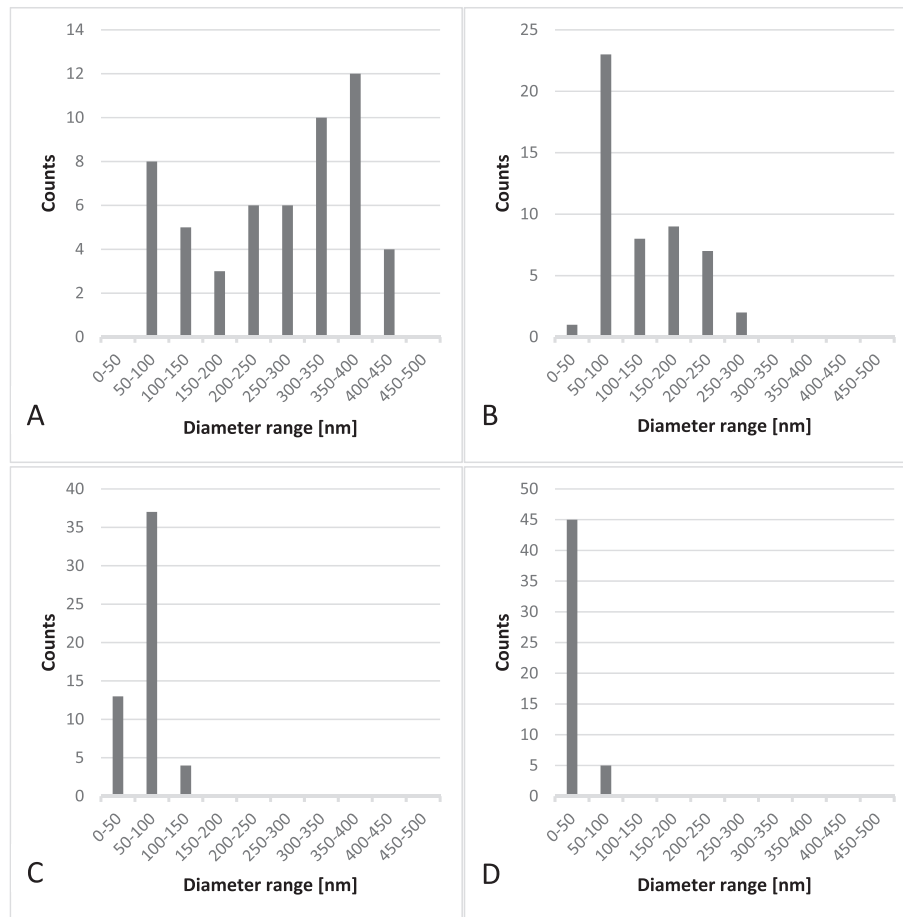


Fig. 3. Histograms of diameters for green composites (A, B) and calcined fibers (C, D) produced from PVA/Th(NO<sub>3</sub>)<sub>4</sub> (A, C) and PVP/Th(acac)<sub>4</sub> (B, D).

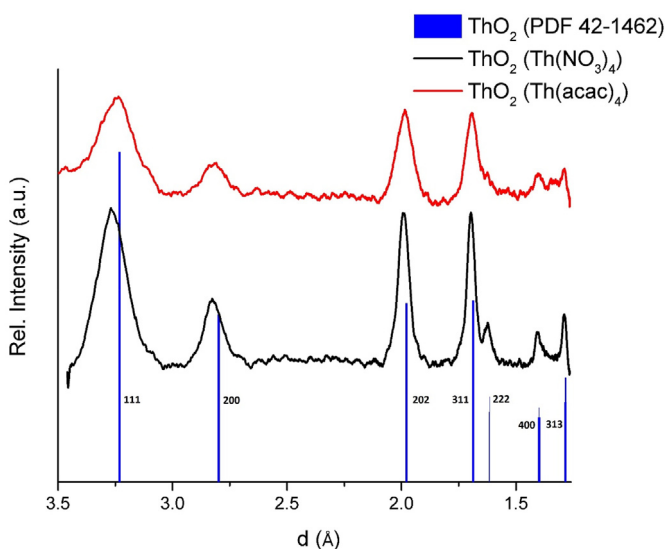


Fig. 4. PXRD measurements of calcined samples. Used lamp Co K $\alpha$  1.79030 Å. X axis: d [Å], Y axis: relative intensity.

the overall process.

In both cases, a white layer of a fibrous material was collected and peeled off the collector. Both materials were analyzed by the TGA/DSC method to obtain information on a proper calcination

temperature (Fig. 1).

Thermogravimetric results revealed the lowest possible temperatures for the complete calcination of the samples. The application of these minimal temperatures is crucial to maintain sample nanocrystalline and small-fiber diameters. The selected temperatures were set at 773 and 673 K for samples A and B, respectively, due to achieving stable mass.

The samples before and after calcination were studied by SEM microscopy (Fig. 2). From a structural point of view, electrospinning of water-based solution produced typical flat ribbon-like fibers, but classical round submicron fibers were also present. These phenomena of ribbon-like fibers formation and its mechanism are well described elsewhere [48]. Also, relatively thick diameters were observed (Fig. 2A) from PVA/Th(NO<sub>3</sub>)<sub>4</sub>, however, with a broad distribution and with two possible maxima observable on the histogram (Fig. 3A). Electrospinning of the organic solution of PVP/Th(acac)<sub>4</sub> produced PVP-containing fibers (Fig. 2B) with a smaller diameter than its aqueous counterpart. Distribution of diameters was less broad (Fig. 3B) than in the previous case, and some part of prepared fibers was already in the nanoscale range.

Calcination of both samples successfully provided the desired inorganic material ThO<sub>2</sub>, which was identified by the PXRD analysis (Fig. 4). Diffractograms in both cases correspond to ThO<sub>2</sub> [PDF 42–1462]; however, individual diffractions were very broad, which corresponds with the nanocrystalline character of these materials. The average diameters of crystallites based on the Scherrer equation and phase compositions correspond in both cases to a cubic ThO<sub>2</sub> phase with 6.9 nm and 6.0 nm sizes for materials resulting

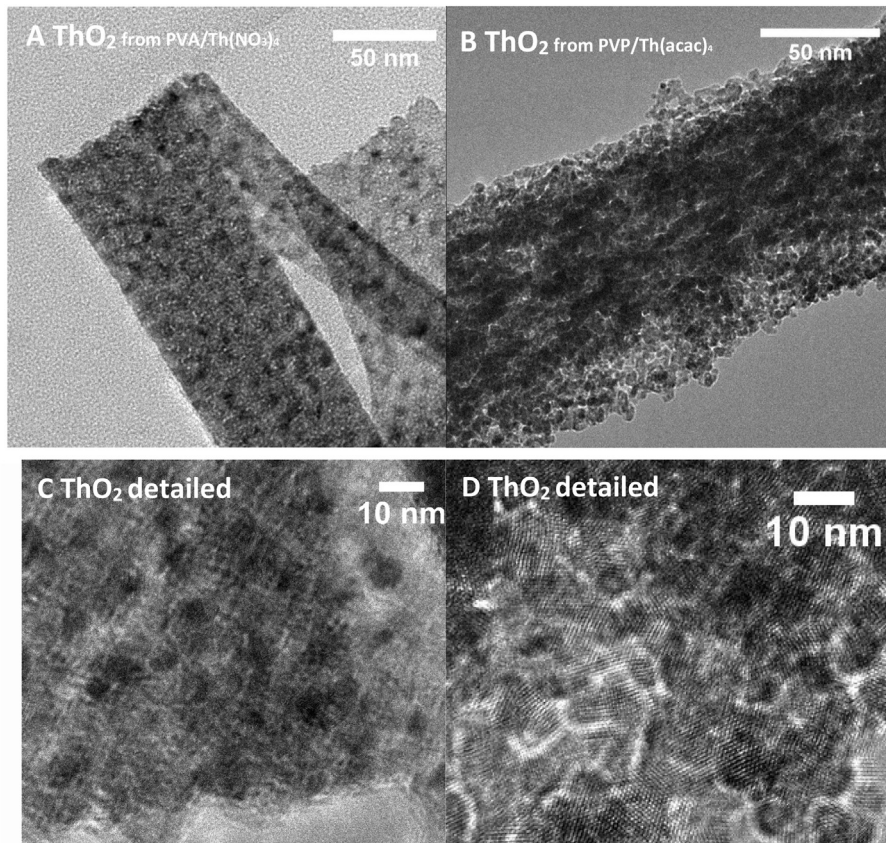


**Fig. 5.** The TEM analysis of calcined products (A, B) with details of nanocrystalline structure (C, D) produced from PVA/Th(NO<sub>3</sub>)<sub>4</sub> (A, C) and PVP/Th(acac)<sub>4</sub> (B, D).

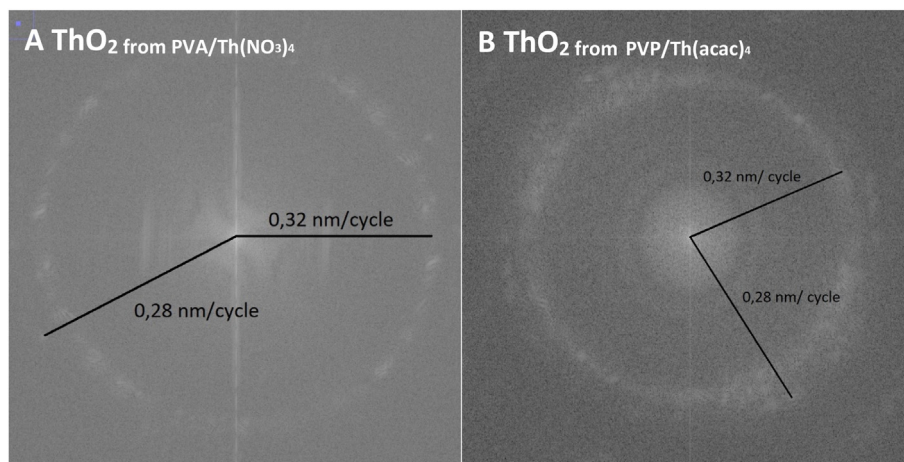


**Fig. 6.** Fast Fourier Transformation analysis of detailed ThO<sub>2</sub> TEM measurements.

from thorium nitrate and acetylacetonate complex, respectively. However, standard deviation of mean coherence lengths is higher than the difference between the two products and therefore it is impossible to differentiate between crystallite sizes. SEM analysis of the calcined sample (Fig. 2C) from PVA/Th(NO<sub>3</sub>)<sub>4</sub> revealed nanofibers with an average diameter of 76 nm and relatively narrow distribution (Fig. 3C). The polycrystalline character of the sample is not observable directly from SEM images. The high-temperature treatment of the sample prepared from the thorium acetylacetonate complex successfully provided ultrathin fibers

(Fig. 2D) with a sharp distribution and diameter smaller than 50 nm in most cases (Fig. 3D). Here also polycrystallinity of the nanofibers was not visible. Due to this fact, TEM analysis was performed to prove overall polycrystallinity and the nanocrystalline character of the prepared materials (Fig. 5).

Detailed TEM analysis was performed by Fast Fourier Transformation for obtaining additional structural data (Fig. 5).

While sample B from thorium acetylacetonate complex shows a clear polycrystalline structure with a diameter of nanocrystallites less than 10 nm (Fig. 5D), sample A (Fig. 5C) shows only crystallinity

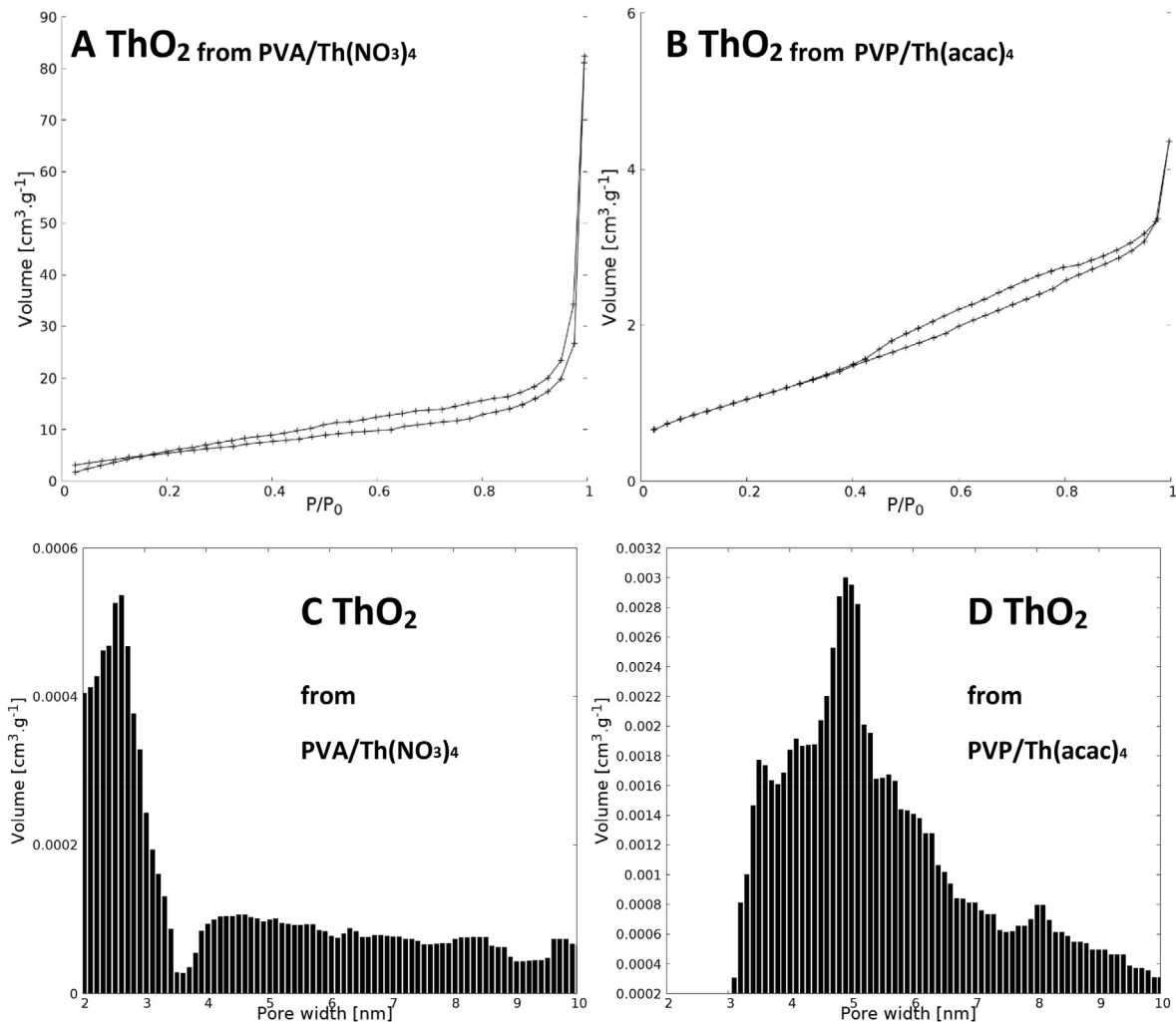


**Fig. 7.** Adsorption/desorption isotherms and corresponding pore size distributions determined by the DFT method of  $\text{ThO}_2$  nanofibers prepared from  $\text{PVA}/\text{Th}(\text{NO}_3)_4$  (A, C) and  $\text{PVP}/\text{Th}(\text{acac})_4$  (B, D).

**Table 3**

Summary of processing and material properties of  $\text{ThO}_2$  nanofibers.

Preparation method	$\text{PVA}/\text{Th}(\text{NO}_3)_4$	$\text{PVP}/\text{Th}(\text{acac})_4$
Feed rate [ $\mu\text{l min}^{-1}$ ]	10	100
Average diameter of green fibers [nm]	$287 \pm 104$	$137 \pm 70$
Average diameter of calcined fibers [nm]	$76 \pm 25$	$34 \pm 18$
Calcination temperature [K]	773	673
Specific surface area [ $\text{m}^2 \text{g}^{-1}$ ]	13	85

observable with a higher magnification. Also, a direct comparison shows that the acetylacetonate-derived fibers show a much more open structure while the nitrate-derived fibers are smoother and more intact on the surface. The Fast Fourier Transformation technique can provide insight into structural properties from observed crystal planes, which should correspond closely to the PXRD measurements. Evaluation of detailed TEM analysis was done by ImageJ software and provided two images (Fig. 6). From both measurements, the formation of two incomplete rings corresponding to crystal planes with distances of 0.32 and 0.28 nm is observable. Those correspond with planes of the Miller indices 111 and 200 (hkl) also found in PXRD measurements of both samples (Fig. 4). The analysis, therefore, indicates the presence of the  $\text{ThO}_2$  phase in its typical  $\text{CaF}_2$  structural type.

The observed open structure of sample B suggested substantial specific surface area. Surface properties and porosity of prepared products were examined by adsorption/desorption isotherms of nitrogen (Fig. 7). In the case of sample A, its BET surface area was  $13 \text{ m}^2 \text{ g}^{-1}$ , the measured isotherm was of Type III of the IUPAC classification [49–51]. The surface area of sample B was  $85 \text{ m}^2 \text{ g}^{-1}$ , its isotherm was also of Type III. Both hysteresis loops suggest large pores. Pore size distribution is in each material different. In the case of thoria produced from thorium nitrate, we can observe two separate maxima (Fig. 7C), while in the other material, it is a continuous distribution with a maximum around 3–4 nm (Fig. 7D). The open structure of sample B from the acetylacetonate complex shows a higher specific surface area than sample A, which was prepared from thorium nitrate/PVA composition. Due to that fact, we can assume that the acetylacetonate complex together with PVP as a supporting polymer is better for final material properties if the material is intended for heterogeneous catalysis applications.

#### 4. Summary and conclusions

In this study, we have achieved the preparation of  $\text{ThO}_2$  in nanofibrous polycrystalline form, which has not been reported in the literature so far. By that we have enlarged spectrum of morphologies with nanocrystalline structure potentially useful as

additive or precursor for fuel manufacturing. However further studies should be done due to unknown sintering properties. Ceramic fibers are traditionally used as reinforcement in composites. Potential application of prepared materials could be found also in that area and preferably in nuclear industry. Other fields for further studies are heterogenous catalysis or development of sorbents due to a relatively high specific surface area. We have developed two synthetic approaches based on different electrospinning solution compositions. Obtained materials differ in their production speed, morphology, and material properties in general (Table 3). ThO<sub>2</sub> prepared from the aqueous solution of thorium nitrate and PVA features thicker fibers with a lower specific surface area. Its counterpart, prepared from thorium acetylacetonate complex and PVP in mixed acetone and ethanol solvents, shows ten times higher electrospinning productivity than the aqueous one based on feed rate during process. After calcination, the material contains ultrafine fibers with an average diameter less than 50 nm. Small diameter, together with an open porous structure, explains a relatively large value of the obtained specific surface area of 85 m<sup>2</sup> g<sup>-1</sup>. Reasons behind different results are based on fundamental distinctions between thoria precursors, used polymers and electrospinning and calcination conditions. The comparison of selected properties is presented in Table 3.

#### Data availability

The raw/processed data required to reproduce these findings cannot be shared at this time as the data also forms part of an ongoing study.

#### Declaration of competing interest

I declare no conflict of interest regarding the manuscript entitled **Preparation of thorium dioxide nanofibers by electrospinning** by Vojtech Kundrat, Zdenek Moravec, and Jiri Pinkas.

#### CRedit authorship contribution statement

**Vojtech Kundrat:** Conceptualization, Investigation, Methodology, Visualization, Writing - original draft. **Zdenek Moravec:** Data curation. **Jiri Pinkas:** Funding acquisition, Resources, Project administration, Supervision, Validation, Writing - review & editing.

#### Acknowledgments

This research has been financially supported by the MEYS CR under the project CEITEC 2020 (LQ1601) and the Horizon 2020 Research and Innovation Program under the grant agreement no. 810626 (SINNCE). CIISB research infrastructure project LM2018127 funded by the MEYS CR is gratefully acknowledged for the financial support of the measurements at the CEITEC MU CF X-ray Diffraction and Bio-SAXS and the CF Cryo-electron Microscopy and Tomography.

#### References

- [1] H.F. Ivey, Candoluminescence and radical-excited luminescence, *J. Lumin.* 8 (1974) 271–307, [https://doi.org/10.1016/0022-2313\(74\)90001-5](https://doi.org/10.1016/0022-2313(74)90001-5).
- [2] C. Ronchi, J.P. Hiernaut, Experimental measurement of pre-melting and melting of thorium dioxide, *J. Alloys Compd.* 240 (1996) 179–185, [https://doi.org/10.1016/0925-8388\(96\)02329-8](https://doi.org/10.1016/0925-8388(96)02329-8).
- [3] F. Cappia, D. Hudry, E. Courtois, A. Janßen, L. Luzzi, R.J.M. Konings, D. Manara, High-temperature and melting behaviour of nanocrystalline refractory compounds: an experimental approach applied to thorium dioxide, *Mater. Res. Express* 1 (2014), <https://doi.org/10.1088/2053-1591/1/2/025034>, 025-034.
- [4] K. Anantharaman, V. Shivakumar, D. Saha, Utilisation of thorium in reactors, *J. Nucl. Mater.* 383 (2008) 119–121, <https://doi.org/10.1016/j.jnucmat.2008.08.042>.
- [5] J.S. Herring, P.E. MacDonald, K.D. Weaver, C. Kullberg, Low cost, proliferation resistant, uranium-thorium dioxide fuels for light water reactors, *Nucl. Eng. Des.* 203 (1) (2001) 65–85, [https://doi.org/10.1016/S0029-5493\(00\)00297-1](https://doi.org/10.1016/S0029-5493(00)00297-1).
- [6] R.K. Sinha, A. Kakodkar, Design and development of the AHWR—the Indian thorium fuelled innovative nuclear reactor, *Nucl. Eng. Des.* 236 (2006) 683–700, <https://doi.org/10.1016/j.nucengdes.2005.09.026>.
- [7] U. Kannan, P.D. Krishnani, Energy from thorium: an Indian perspective, *Sadhana* 38 (5) (2013) 817–837.
- [8] V. Tyrpekl, M. Cologna, D. Robba, J. Somers, Sintering behaviour of nanocrystalline ThO<sub>2</sub> powder using spark plasma sintering, *J. Eur. Ceram. Soc.* 36 (2016) 767–772, <https://doi.org/10.1016/j.jeurceramsoc.2015.11.006>.
- [9] F. Righini, J. Spišiak, G.C. Bussolino, A. Rosso, G.K. White, Thermophysical properties of thoriated tungsten above 3600 K by a pulse-heating method, *Int. J. Thermophys.* 17 (1996) 1025–1036, <https://doi.org/10.1007/BF01441991>.
- [10] G. Jacobs, A. Crawford, L. Williams, P.M. Patterson, B.H. Davis, Low temperature water–gas shift: comparison of thoria and ceria catalysts, *Appl. Catal. Gen.* 267 (2004) 27–33, <https://doi.org/10.1016/j.apcata.2004.02.021>.
- [11] T. Tabakova, V. Idakiev, K. Tenchev, F. Boccuzzi, M. Manzoli, A. Chiorini, Pure hydrogen production on a new gold–thoria catalyst for fuel cell applications, *Appl. Catal. B Environ.* 63 (2006) 94–103, <https://doi.org/10.1016/j.apcatb.2005.09.017>.
- [12] T. Baidya, N. van Vegten, Y. Jiang, F. Krumeich, A. Baiker, Oxidative coupling of methane over Ca- and alkali metal-doped ThO<sub>2</sub>, *Appl. Catal. Gen.* 391 (2011) 205–214, <https://doi.org/10.1016/j.apcata.2010.03.058>.
- [13] C. Suryanarayana, Nanocrystalline materials, *Int. Mater. Rev.* 40 (1995) 41–64, <https://doi.org/10.1179/imr.1995.40.2.41>.
- [14] O. Guillon, J. Gonzalez-Julian, B. Dargatz, T. Kessel, G. Schierning, J. Räthel, M. Herrmann, Field-assisted sintering technology/spark plasma sintering: mechanisms, materials, and technology developments: FAST/SPS: mechanisms, materials, and technology developments, *Adv. Eng. Mater.* 16 (2014) 830–849, <https://doi.org/10.1002/adem.201300409>.
- [15] M.J. Mayo, Processing of nanocrystalline ceramics from ultrafine particles, *Int. Mater. Rev.* 41 (1996) 85–115, <https://doi.org/10.1179/imr.1996.41.3.85>.
- [16] S.E. Pratsinis, Flame aerosol synthesis of ceramic powders, *Prog. Energy Combust. Sci.* 24 (1998) 197–219, [https://doi.org/10.1016/S0360-1285\(97\)00028-2](https://doi.org/10.1016/S0360-1285(97)00028-2).
- [17] B.L. Cushing, V.L. Kolesnichenko, C.J. O'Connor, Recent advances in the liquid-phase syntheses of inorganic nanoparticles, *Chem. Rev.* 104 (2004) 3893–3946, <https://doi.org/10.1021/cr030027b>.
- [18] N. Lewinski, V. Colvin, R. Drezek, Cytotoxicity of nanoparticles, *Small* 4 (2008) 26–49, <https://doi.org/10.1002/sml.200700595>.
- [19] T. Yousefi, M. Torab-Mostaedi, H. Sohbatazadeh, A.R. Keshtkar, H. Aghayan, M.G. Maragheh, Synthesis and characterization of ultra-fine well-dispersed thoria nano spheres through reduction reactions in nitrate bath, *Prog. Nucl. Energy* 85 (2015) 600–604, <https://doi.org/10.1016/j.pnucene.2015.08.002>.
- [20] V.K. Tripathi, R. Nagarajan, Sol–gel synthesis of high-purity actinide oxide ThO<sub>2</sub> and its solid solutions with technologically important tin and zinc ions, *Inorg. Chem.* 55 (2016) 12798–12806, <https://doi.org/10.1021/acs.inorgchem.6b02086>.
- [21] N. Mohseni, S.J. Ahmadi, M. Roshanzamir, M. Najafi, S.M. Mirvakili, Characterization of ThO<sub>2</sub> and (Th,U)O<sub>2</sub> pellets consolidated from NSD-sol gel derived nanoparticles, *Ceram. Int.* 43 (2017) 3025–3034, <https://doi.org/10.1016/j.ceramint.2016.11.096>.
- [22] P. Cakir, R. Eloiroid, F. Huber, R.J.M. Konings, T. Gouder, An XPS and UPS study on the electronic structure of ThO<sub>x</sub> (x ≤ 2) thin films, *J. Phys. Chem. C* 118 (2014) 24497–24503, <https://doi.org/10.1021/jp506750p>.
- [23] R.A. Reibold, J.F. Poco, T.F. Baumann, R.L. Simpson, J.H. Satcher, Synthesis and characterization of a nanocrystalline thoria aerogel, *J. Non-Cryst. Solids* 341 (2004) 35–39, <https://doi.org/10.1016/j.jnocrsol.2004.05.008>.
- [24] D. Sanjay Kumar, K. Ananthasivan, S. Amirthapandian, A. Dasgupta, G. Jogeswara Rao, Citrate gel-combustion synthesis and sintering of nanocrystalline ThO<sub>2</sub> powders, *J. Nucl. Mater.* 497 (2017) 16–29, <https://doi.org/10.1016/j.jnucmat.2017.10.006>.
- [25] R.D. Purohit, S. Saha, A.K. Tyagi, Nanocrystalline thoria powders via glycine-nitrate combustion, *J. Nucl. Mater.* 288 (2001) 7–10, [https://doi.org/10.1016/S0022-3115\(00\)00717-0](https://doi.org/10.1016/S0022-3115(00)00717-0).
- [26] S. Dash, M. Kamruddin, P.K. Ajikumar, A.K. Tyagi, B. Raj, S. Bera, S.V. Narasimhan, Temperature programmed decomposition of thorium nitrate pentahydrate, *J. Nucl. Mater.* 278 (2000) 173–185, [https://doi.org/10.1016/S0022-3115\(99\)00261-5](https://doi.org/10.1016/S0022-3115(99)00261-5).
- [27] V. Tyrpekl, J.-F. Vigier, D. Manara, T. Wiss, O. Dieste Blanco, J. Somers, Low temperature decomposition of U(IV) and Th(IV) oxalates to nanograined oxide powders, *J. Nucl. Mater.* 460 (2015) 200–208, <https://doi.org/10.1016/j.jnucmat.2015.02.027>.
- [28] V. Chandramouli, S. Anthonysamy, P.R. Vasudeva Rao, R. Divakar, D. Sundararaman, PVA aided microwave synthesis: a novel route for the production of nanocrystalline thoria powder, *J. Nucl. Mater.* 231 (1996) 213–220, [https://doi.org/10.1016/0022-3115\(96\)00368-6](https://doi.org/10.1016/0022-3115(96)00368-6).
- [29] L. Wang, R. Zhao, X. Wang, L. Mei, L. Yuan, S. Wang, Z. Chai, W. Shi, Size-tunable synthesis of monodisperse thorium dioxide nanoparticles and their performance on the adsorption of dye molecules, *CrystEngComm* 16 (2014) 10469–10475, <https://doi.org/10.1039/C4CE001731E>.
- [30] R. Zhao, L. Wang, Z.-F. Chai, W.-Q. Shi, Synthesis of ThO<sub>2</sub> nanostructures through a hydrothermal approach: influence of hexamethylenetetramine

- (HMTA) and sodium dodecyl sulfate (SDS), RSC Adv. 4 (2014) 52209–52214, <https://doi.org/10.1039/C4RA07466A>.
- [31] N. Clavier, J. Maynadié, A. Mesbah, J. Hidalgo, R. Lauwerier, G.I. Nkou Bouala, S. Parrès-Maynadié, D. Meyer, N. Dacheux, R. Podor, Thorium aspartate tetrahydrate precursor to ThO<sub>2</sub> : comparison of hydrothermal and thermal conversions, J. Nucl. Mater. 487 (2017) 331–342, <https://doi.org/10.1016/j.jnucmat.2017.02.035>.
- [32] D. Hudry, C. Apostolidis, O. Walter, T. Gouder, E. Courtois, C. Kübel, D. Meyer, Non-aqueous synthesis of isotropic and anisotropic actinide oxide nanocrystals, Chem. Eur J. 18 (2012) 8283–8287, <https://doi.org/10.1002/chem.201200513>.
- [33] D. Hudry, C. Apostolidis, O. Walter, T. Gouder, E. Courtois, C. Kübel, D. Meyer, Controlled synthesis of thorium and uranium oxide nanocrystals, Chem. Eur J. 19 (2013) 5297–5305, <https://doi.org/10.1002/chem.201203888>.
- [34] R. Ramaseshan, S. Sundarajan, R. Jose, S. Ramakrishna, Nanostructured ceramics by electrospinning, J. Appl. Phys. 102 (2007), <https://doi.org/10.1063/1.2815499>, 111–101.
- [35] Y. Dai, W. Liu, E. Formo, Y. Sun, Y. Xia, Ceramic nanofibers fabricated by electrospinning and their applications in catalysis, environmental science, and energy technology, Polym. Adv. Technol. 22 (2011) 326–338, <https://doi.org/10.1002/pat.1839>.
- [36] H. Wu, W. Pan, D. Lin, H. Li, Electrospinning of ceramic nanofibers: fabrication, assembly and applications, J. Adv. Ceram. 1 (2012) 2–23, <https://doi.org/10.1007/s40145-012-0002-4>.
- [37] V. Kundrat, A. Patak, J. Pinkas, Preparation of ultrafine fibrous uranium dioxide by electrospinning, J. Nucl. Mater. 528 (2020) 151877, <https://doi.org/10.1016/j.jnucmat.2019.151877>.
- [38] D. Li, Y. Xia, Electrospinning of nanofibers: reinventing the wheel? Adv. Mater. 16 (2004) 1151–1170, <https://doi.org/10.1002/adma.200400719>.
- [39] R.C. Young, J. Kovitz, L.E. Marchi, Thorium acetylacetonate (Tetrakis(2,4-Pentanedionato)Thorium), in: W.C. Ferneliuss (Ed.), Inorganic Syntheses, John Wiley & Sons, Inc., Hoboken, NJ, USA, 2007, pp. 123–125, <https://doi.org/10.1002/9780470132333.ch36>.
- [40] R. Bardestani, G.S. Patience, S. Kaliaguine, Experimental methods in chemical engineering: specific surface area and pore size distribution measurements—BET, BJH, and DFT, Can. J. Chem. Eng. 97 (2019) 2781–2791, <https://doi.org/10.1002/cjce.23632>.
- [41] P.A. Monson, Understanding adsorption/desorption hysteresis for fluids in mesoporous materials using simple molecular models and classical density functional theory, Microporous Mesoporous Mater. 160 (2012) 47–66, <https://doi.org/10.1016/j.micromeso.2012.04.043>.
- [42] A. Koski, K. Yim, S. Shivkumar, Effect of molecular weight on fibrous PVA produced by electrospinning, Mater. Lett. 58 (2004) 493–497, [https://doi.org/10.1016/S0167-577X\(03\)00532-9](https://doi.org/10.1016/S0167-577X(03)00532-9).
- [43] C. Zhang, X. Yuan, L. Wu, Y. Han, J. Sheng, Study on morphology of electrospun poly(vinyl alcohol) mats, Eur. Polym. J. 41 (2005) 423–432, <https://doi.org/10.1016/j.eurpolymj.2004.10.027>.
- [44] C. Shao, H.-Y. Kim, J. Gong, B. Ding, D.-R. Lee, S.-J. Park, Fiber mats of poly(vinyl alcohol)/silica composite via electrospinning, Mater. Lett. 57 (2003) 1579–1584, [https://doi.org/10.1016/S0167-577X\(02\)01036-4](https://doi.org/10.1016/S0167-577X(02)01036-4).
- [45] M. Bognitzki, T. Frese, M. Steinhart, A. Greiner, J.H. Wendorff, A. Schaper, M. Hellwig, Preparation of fibers with nanoscaled morphologies: electrospinning of polymer blends, Polym. Eng. Sci. 41 (2001) 982–989, <https://doi.org/10.1002/pen.10799>.
- [46] H. Pan, L. Li, L. Hu, X. Cui, Continuous aligned polymer fibers produced by a modified electrospinning method, Polymer 47 (2006) 4901–4904, <https://doi.org/10.1016/j.polymer.2006.05.012>.
- [47] Q. Yang, Z. Li, Y. Hong, Y. Zhao, S. Qiu, C. Wang, Y. Wei, Influence of solvents on the formation of ultrathin uniform poly(vinyl pyrrolidone) nanofibers with electrospinning, J. Polym. Sci., Polym. Phys. Ed. 42 (2004) 3721–3726, <https://doi.org/10.1002/polb.20222>.
- [48] S. Ramakrishna, K. Fujihara, W.-E. Teo, T.-C. Lim, Z. Ma, An Introduction to Electrospinning and Nanofibers, 2005, <https://doi.org/10.1142/5894>. WORLD SCIENTIFIC.
- [49] Z. Allothman, A review: fundamental aspects of silicate mesoporous materials, Materials 5 (2012) 2874–2902, <https://doi.org/10.3390/ma5122874>.
- [50] F. Rouquerol, J. Rouquerol, K. Sing, Adsorption by Powders and Porous Solids, Academic Press, London, 1999.
- [51] S. Lowell, J.E. Shields, M.A. Thomas, M. Thommes, Characterization of Porous Solids and Powders, Kluwer Academic Publishers, Dordrecht, 2004.